



Scaling of Resistance and Electron Mean Free Path of Single-Walled Carbon Nanotubes

Meninder S. Purewal,¹ Byung Hee Hong,² Anirudhh Ravi,² Bhupesh Chandra,³ James Hone,³ and Philip Kim²

¹*Department of Applied Physics and Applied Math, Columbia University, New York, New York 10027, USA*

²*Department of Physics, Columbia University, New York, New York 10027, USA*

³*Department of Mechanical Engineering, Columbia University, New York, New York 10027, USA*

(Received 25 January 2007; published 4 May 2007)

We present an experimental investigation on the scaling of resistance in individual single-walled carbon nanotube devices with channel lengths that vary 4 orders of magnitude on the same sample. The electron mean free path is obtained from the linear scaling of resistance with length at various temperatures. The low temperature mean free path is determined by impurity scattering, while at high temperature, the mean free path decreases with increasing temperature, indicating that it is limited by electron-phonon scattering. An unusually long mean free path at room temperature has been experimentally confirmed. Exponentially increasing resistance with length at extremely long length scales suggests anomalous localization effects.

DOI: [10.1103/PhysRevLett.98.186808](https://doi.org/10.1103/PhysRevLett.98.186808)

PACS numbers: 73.63.-b, 73.22.-f, 73.23.-b

Single-walled carbon nanotubes (SWNTs) are 1D conductors that exhibit a rich variety of low dimensional charge transport phenomena [1], including ballistic conduction [2–6], localization [7], and 1D variable range hopping [8]. The electron mean free path, L_m , is one of the important length scales that characterize the different 1D transport regimes. One method of determining L_m in SWNTs is to measure ballistic conduction for a given device channel length. However, this method yields a lower bound of L_m , and works only at low temperature [2–5] or at higher temperature for small length scales (<60 nm) [6]. Another approach to obtain L_m at room temperature is to employ scanning probe microscopy to measure the linear scaling of the channel resistance [9] or use noninvasive multiterminal measurements [10]. Because of the experimental limitations of these approaches, the characterization of L_m for the same SWNTs over a range of temperatures is yet to be realized.

Recent advances in the growth of extremely long SWNTs (>1 mm) [11] now allow for an intensive study on their intrinsic properties. In this Letter, we present experimental measurements on the scaling behavior of resistance in individual, millimeter long SWNTs for the temperature range of 1.6–300 K. From the linear scaling of resistance, the temperature dependent electron mean free path is calculated for each temperature. Beyond the linear scaling regime, we observe that the resistance increases exponentially with length, indicating localization behavior.

Macroscopically long and straight individual SWNTs were grown on a degenerately doped Si/SiO₂ substrate ($t_{\text{ox}} = 500$ nm) using the chemical vapor deposition method described in Ref. [11]. This was followed by the fabrication of multiple Pd electrodes with various separations (200 nm – 400 μm) (Fig. 1(a)). Pd electrodes were chosen to create highly transparent SWNT-electrode contacts [4]. The diameters of the SWNTs were measured by atomic force microscope (AFM). We chose SWNTs with

diameter d less than 2.5 nm to exclude any possibility of including multiwalled nanotubes (MWNT) in this study. In addition, we confirmed that the high bias saturation current is <30 μA for all SWNTs studied [12], assuring that the samples consisted of single tubes rather than small bundles or MWNTs. The substrate was used as a gate electrode to tune the chemical potential of the sample by the application of a gate voltage V_g . A small dc source-drain bias voltage (<10 mV), V_{SD} , was applied between pairs of consecutive electrodes, and the two-terminal linear response conductance was determined from the measured source-drain current I_{SD} .

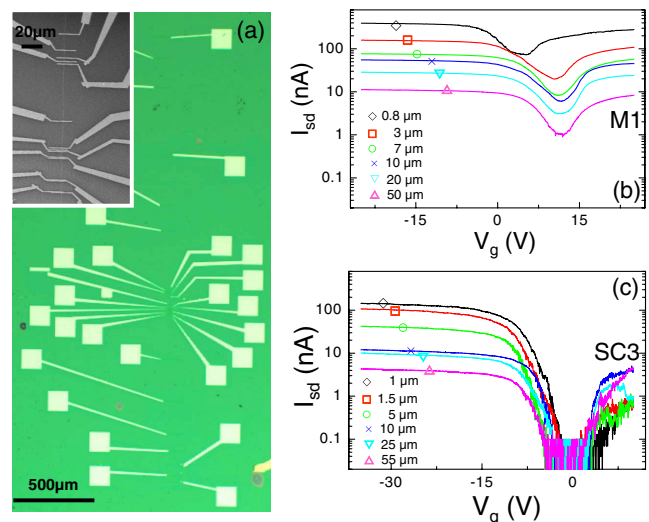


FIG. 1 (color online). (a) Optical image showing typical SWNT devices with multiple Pd electrodes. (Inset) Scanning electron microscope image of an isolated SWNT contacted with these electrodes. Room temperature $I_{\text{SD}}(V_g)$ of selected channel lengths for (b) metallic SWNT (M1) and (c) semiconducting SWNT (SC3) with $V_{\text{SD}} = 6.4$ and 2.7 mV, respectively.

Figures 1(b) and 1(c) show the measured I_{SD} as a function of V_{SD} for selected channel length sections on two representative SWNTs. All curves exhibit a “gap” like feature—a range of V_g where I_{SD} is suppressed. On the same SWNT, every device (pair of consecutive electrodes) shows a similar $I_{SD}(V_g)$ up to a length-dependent multiplicative factor, once we align the centers of the gap region for each curve. The similarity of the $I_{SD}(V_g)$ behavior in different sections for each SWNT sample indicates that the corresponding “gap” features are derived from the intrinsic electronic structure of the SWNT rather than the effects of random local variation.

We use the qualitatively different $I_{SD}(V_g)$ behaviors of different SWNTs to categorize them as metallic (M-NT) or semiconducting nanotubes (S-NT). Typical S-NTs (Fig. 1(c)) exhibit an off current region $I_{SD} < 10^{-10}$ A when the Fermi energy E_F lies in the energy gap [13,14]. On the other hand, a weaker suppression of $I_{SD}(V_g)$ is observed in the “small gap” region in M-NTs (Fig. 1(b)). The “small gap” in M-NTs has been attributed to the curvature-induced energy gap $E_g < 100$ meV [15], which is distinguished from the S-NT energy gap, which scales with diameter as $E_g \sim 1/d$ (nm) [1]. Among the 11 SWNTs we studied in this Letter, we found 4 M-NTs and 7 S-NTs. Each of these SWNTs exhibit a gap centered at $V_g > 0$, indicating their p -doped nature. At large negative gate voltage ($V_g < -20$ V), E_F lies well outside of the gap region and $I_{SD}(V_g)$ saturates to I_{SD}^{sat} , whose value depends only on the applied V_{SD} and channel length L of the SWNT section. The two-terminal resistance of the SWNT section is then obtained from $R(L) = V_{SD}/I_{SD}^{sat}$. We note that four-terminal resistance measurements are possible for each section by utilizing the available multiple electrode configuration. However, in our experiment, the four-terminal measurements yield essentially similar results to the two-terminal $R(L)$, which prevents separation of the “contact” resistance contribution from $R(L)$. Such inseparable contact resistance between SWNT-metal electrodes was reported to be caused by the invasiveness of metal contacts [16].

We designed many pairs of electrodes with different L on each SWNT so that the scaling of $R(L)$ can be studied for a specific sample at a given temperature T . Figure 2(a) shows $R(L)$ of a representative SWNT measured in the temperature range of 1.6–300 K and with an L range of 200 nm – 50 μ m. In these ranges, $R(L)$ increases linearly and appears to converge to a finite value for small L (inset to Fig. 2(a)). We found that this scaling behavior can be described well by a simple linear dependence with an offset: $R(L) = \rho L + R_c$, where ρ and R_c are interpreted as the 1D resistivity and contact resistance, respectively. The solid lines in Fig. 2(a) are the two parameter line fits of the data points at a given T value. From these fits, $R_c(T)$ and $\rho(T)$ are obtained as shown in Figs. 2(b) and 2(c), respectively. For this sample, R_c remains fairly constant at

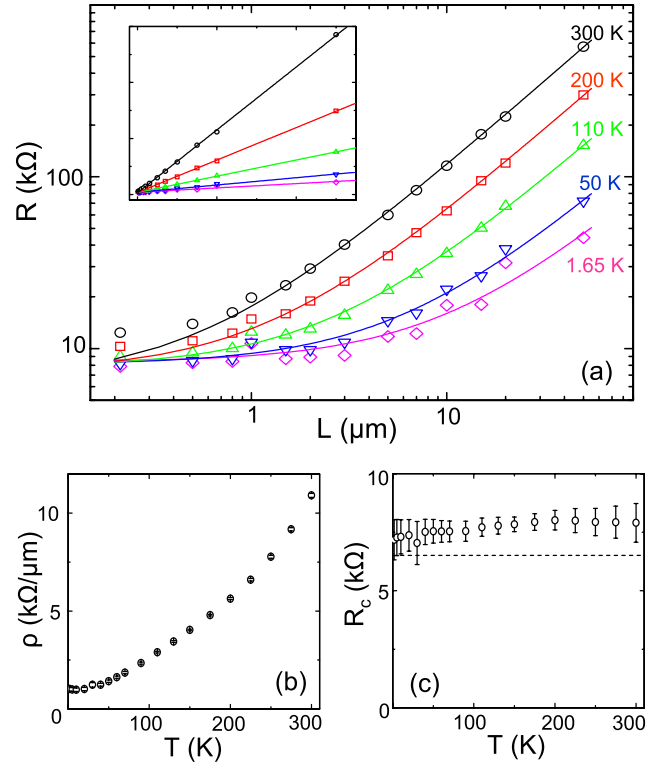


FIG. 2 (color online). (a) (Inset) $R(L)$ for sample M1 at select temperatures ranging from 1.6–300 K. (Main) A log-log plot highlights the behaviors at different lengths scaling 3 orders of magnitude. From the linear fits (solid lines) of these data points, we obtain the 1D resistivity (b) and the contact resistance (c) at different temperatures. The dashed line in (c) represents R_Q .

~ 8 k Ω , and $\rho(T)$ exhibits typical metallic behavior; i.e., it decreases with T and saturates to a value ρ_{sat} at low temperatures. Similar scaling behavior of $R(L)$ is observed in other SWNTs, from which both R_c and $\rho(T)$ are extracted within the linear scaling regime. Table I summarizes d , R_c , and ρ_{sat} for the 4 M-NTs and 7 S-NTs considered in this Letter. To understand the scaling of $R(L)$ in Fig. 2, we begin with the two-terminal Landauer-Buttiker formula applied to SWNTs [9]. If we consider 4 low-energy channels in the SWNT, 2 each for spin and band degeneracy, then the scaling of resistance is given by $R(L) = (h/4e^2)(L/L_m + 1) + R_{nc}$, where e and h are electron charge and Planck constant and L_m and R_{nc} are the electron mean free path and the nontransparent contact resistance, respectively. Note that we separate out the contribution of R_{nc} from the total contact resistance R_c , so that the contact resistance becomes the quantum resistance $R_Q = h/4e^2$ when the contacts become fully transparent. From the experimentally obtained $\rho(T)$ and R_c , we can deduce $L_m = R_Q/\rho(T)$ and $R_{nc} = R_c - R_Q$ for each of our SWNT samples. In particular, we note that $R_{nc} \lesssim R_Q$ for the majority of our samples, suggesting that the barrier at the contacts is very thin and adds only a negligible contribution when L becomes substantially large.

TABLE I. Device characteristics for SWNTs used in this Letter. The character M (SC) is designated for metallic (semiconducting) SWNTs.

	M1	M2	M3	M4	SC1	SC2	SC3	SC4	SC5	SC6	SC7
$d(\text{nm})$	$2.0 \pm .2$	$1.3 \pm .4$	$1.7 \pm .6$	$1.6 \pm .4$	$1.6 \pm .4$	$1.8 \pm .6$	$1.9 \pm .4$	$2.1 \pm .2$	$2.2 \pm .2$	$2.0 \pm .6$	$2.2 \pm .2$
$R_c(\text{k}\Omega)$	$7.9 \pm .8$	11.5 ± 2.9	8.3 ± 2.5	12.0 ± 4.4	10.2 ± 4.5	14.9 ± 5.7	$10.4 \pm .9$	7.0 ± 2.3	25.4 ± 4.2	6.9 ± 40	21.8 ± 14
$\rho_{\text{sat}}(\text{k}\Omega/\mu\text{m})$	$0.76 \pm .02$	$0.87 \pm .02$	$0.93 \pm .01$	$6.5 \pm .08$	$2.95 \pm .05$	$3.61 \pm .05$	$4.64 \pm .01$	$5.91 \pm .12$	$8.13 \pm .31$	$14.1 \pm .19$	$16.3 \pm .13$
$L_m^{\text{sat}}(\mu\text{m})$	$8.56 \pm .23$	$7.65 \pm .17$	$7.07 \pm .08$	$1.00 \pm .01$	$2.24 \pm .04$	$1.83 \pm .03$	$1.40 \pm .01$	$1.10 \pm .02$	$0.80 \pm .03$	$0.47 \pm .01$	$0.40 \pm .01$

We now discuss the temperature dependent behavior of the mean free path. Figure 3 is the central result of this Letter, showing $L_m(T)$ of the SWNTs listed in Table I. Overall, $L_m(T)$ exhibits different behaviors in two regimes separated by T_{cr} : (i) the high temperature regime ($T > T_{\text{cr}}$) where $L_m \sim T^{-1}$ (dashed line in Fig. 3), which indicates that inelastic scattering between electrons and acoustic phonons is dominant [9,17] regardless of chirality [18]; and (ii) the low temperature regime ($T < T_{\text{cr}}$) where L_m saturates to the tube specific L_m^{sat} . In this low temperature limit, the phonons freeze out and L_m^{sat} is determined by the temperature independent elastic scattering with impurities. We believe the widely spread L_m^{sat} values (0.4–10 μm) in (ii) are a result of each SWNT sample having a static disorder of different strengths and densities. We employ scanning gate microscopy (SGM) [19] to image this static disorder. Indeed, the SGM images on S-NTs (insets to Fig. 3) reveal that the SWNT with a shorter L_m^{sat} shows more defects. Note also that we have experimentally confirmed that L_m is generally much higher for M-NTs than that of S-NTs. This is an indication that the scattering of electrons is strongly suppressed in M-NTs, as predicted by Ando *et al.* [20] and McEuen *et al.* [21]. In M-NTs, we have experimentally shown that the ballistic electron conduction is possible for channel lengths up to 8 μm at low temperature and 0.8 μm even at room temperature.

Finally, we turn our attention to the nonlinear scaling of $R(L)$. Figure 4 presents $R(L)$ beyond the linear scaling regime of a representative S-NT and M-NT. At extremely long length scales and low temperatures, $R(L)$ deviates from the linear dependence extended from the linear regime (dashed lines in main figure and see also $R_{\text{dev}} = R(L) - R_c - R_Q L/L_m$ in lower insets). Since $R(L \ll L_m^{\text{sat}}) \sim R_Q$ for all temperatures, we emphasize here that this nonlinear behavior in $R(L)$ is solely due to increasing electron scattering in the bulk part of the SWNTs rather than an increasing barrier between the SWNT and electrodes. In order to experimentally determine the critical length scale L_c beyond which the nonlinear behaviors are dominant, we use a phenomenological equation: $R(L) = R_c + R_Q(L/L_m + e^{L/L_c})$ to fit the data (solid curves in Fig. 4). While L_c shows a strong sample dependent behavior, generally we found $L_c \gg L_m$ in all temperature ranges, with the temperature dependence exhibiting a trend of increasing L_c with increasing T (upper insets to Fig. 4).

This observed behavior of $L_c(T)$ excludes the quantum interference related to strong localization effects such as Anderson Localization [7] from the possible scenarios. In particular, in the high temperature regime ($T > T_{\text{cr}}$), the phase coherence length L_ϕ is limited by the phase-breaking electron-phonon scattering, and thus $L_\phi \sim L_m \ll L_c$, inviting further study to elucidate the observed localization behavior beyond the strong localization limit [22,23].

In conclusion, we determine the length-dependent resistance for SWNTs with channel lengths ranged 200 nm – 400 μm . From the scaling behavior, we evaluate the electron mean free path and localization length of the SWNT for a range of temperatures. While the low temperature mean free path is determined by the impurity scattering, an unusually long mean free path is demon-

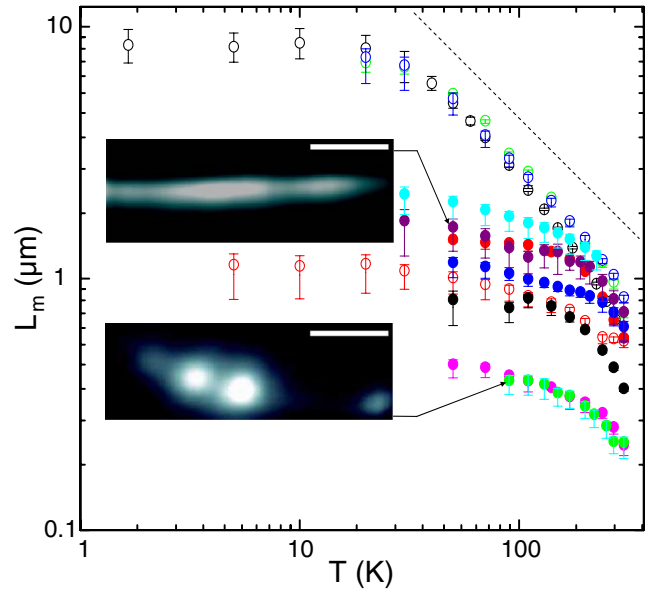


FIG. 3 (color online). The electron mean free path for the samples listed in Table I at different temperatures. Most metallic SWNTs (open circles) saturate at higher values than that of semiconductors (closed circles). The dashed line represents T^{-1} dependence. The insets show scanning gate microscopy images taken on devices SC2 (upper) and SC7 (lower). Lighter color corresponds less current in the SWNT. The defects in the SWNT are highlighted by the bright region (suppressed current) on the SWNT. The scale bar is 500 nm.

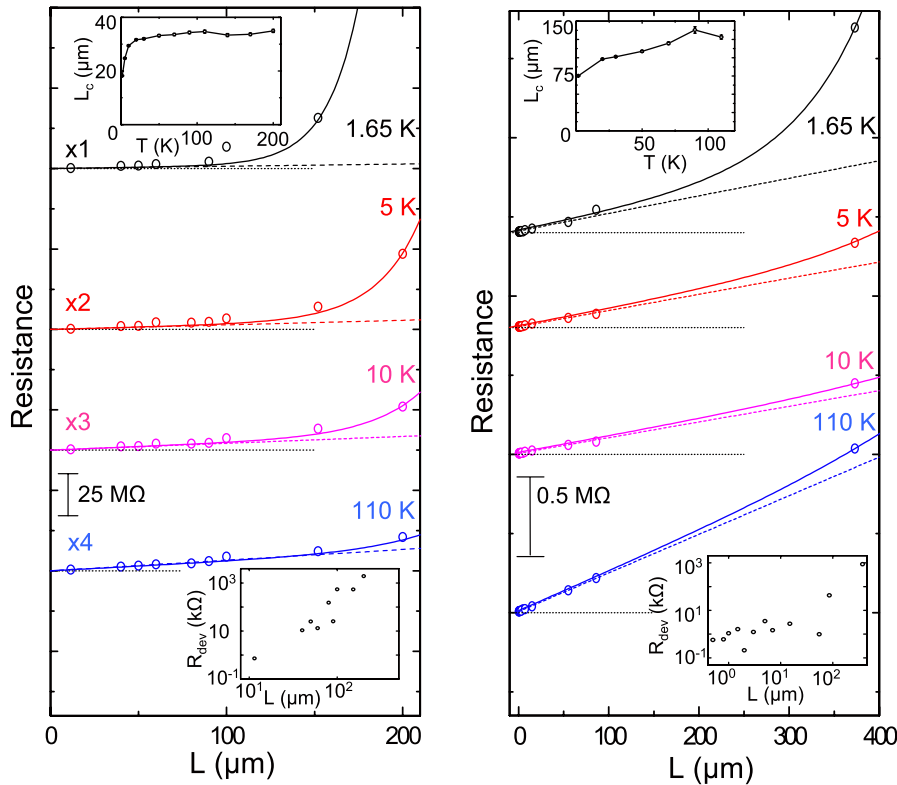


FIG. 4 (color online). $R(L)$ in the non-linear regimes for samples (a) SC6 ($L_m^{\text{sat}} \approx 460 \text{ nm}$) and (b) M3 ($L_m^{\text{sat}} \approx 7 \mu\text{m}$). Note that the data are magnified in (a) for clarity. The dashed line is an extension of the linear regime, and the solid line is a fit for all data. R_{dev} shows the absolute value of the difference between the actual device resistance and the corresponding linear resistance at 110 K (lower inset a) and 1.65 K (lower inset b). The nonlinearity increases with decreasing temperature, which is reflected in the value of L_c (upper insets).

strated at room temperature, even with the dominant electron-phonon scattering.

We thank I. Aleiner, B. Altshuler, and P. Jarillo-Herrero for helpful discussions. This work is supported by the NSF No. NIRT(ECS 0507111), CAREER (No. DMR-0349232), NSEC (No. CHE-0117752), and the New York State Office of Science, Technology, and Academic Research (NYSTAR).

- [1] R. Saito, G. Dresselhaus, and M. S. Dresselhaus, *Physical Properties of Carbon Nanotubes* (Imperial College Press, London, 1998).
- [2] J. Kong, E. Yenilmez, T.W. Tomblor, W. Kim, H. Dai, R. B. Laughlin, L. Liu, C. S. Jayanthi, and S. Y. Wu, *Phys. Rev. Lett.* **87**, 106801 (2001).
- [3] W. Liang, M. Bockrath, D. Bozovic, J.H. Hafner, M. Tinkham, and H. Park, *Nature (London)* **411**, 665 (2001).
- [4] D. Mann, A. Javey, J. Kong, Q. Wang, and H. Dai, *Nano Lett.* **3**, 1541 (2003).
- [5] A. Javey, J. Guo, Q. Wang, M. Lundstrom, and H. Dai, *Nature (London)* **424**, 654 (2003).
- [6] A. Javey, J. Guo, M. Paulsson, Q. Wang, D. Mann, M. Lundstrom, and H. Dai, *Phys. Rev. Lett.* **92**, 106804 (2004).
- [7] C. Gomez-Navarro, P.J. de Pablo, J. Gomez-Herrero, B. Biel, F.J. Garcia-Vidal, A. Rubio, and F. Flores, *Nat. Mater.* **4**, 534 (2005).
- [8] B. Gao, D.C. Glattli, B. Placais, and A. Bachtold, *Phys. Rev. B* **74**, 085410 (2006).
- [9] J. Park, S. Rosenblatt, Y. Yaish, V. Sazonova, H. Ustunel, S. Braig, T. A. Arias, P.W. Brouwer, and P.L. McEuen, *Nano Lett.* **4**, 517 (2004).
- [10] B. Gao, Y.F. Chen, M.S. Fuhrer, D.C. Glattli, and A. Bachtold, *Phys. Rev. Lett.* **95**, 196802 (2005).
- [11] B.H. Hong, J. Y. Lee, T. Beetz, Y. Zhu, P. Kim, and K. S. Kim, *J. Am. Chem. Soc.* **127**, 15336 (2005).
- [12] Z. Yao, C.L. Kane, and C. Dekker, *Phys. Rev. Lett.* **84**, 2941 (2000).
- [13] S.J. Tans, A.R.M. Verschueren, and C. Dekker, *Nature (London)* **393**, 49 (1998).
- [14] J. Appenzeller, J. Knoch, V. Derycke, R. Martel, S. Wind, and Ph. Avouris, *Phys. Rev. Lett.* **89**, 126801 (2002).
- [15] C. Zhou, J. Kong, and H. Dai, *Phys. Rev. Lett.* **84**, 5604 (2000).
- [16] A. Bezryadin, A.R.M. Verschueren, S.J. Tans, and C. Dekker, *Phys. Rev. Lett.* **80**, 4036 (1998).
- [17] V. Perebeinos, J. Tersoff, and Ph. Avouris, *Phys. Rev. Lett.* **94**, 086802 (2005).
- [18] X. Zhou, J. Park, S. Huang, J. Liu, and P.L. McEuen, *Phys. Rev. Lett.* **95**, 146805 (2005).
- [19] A. Bachtold, M. S. Fuhrer, S. Plyasunov, M. Forero, E. H. Anderson, A. Zettl, and P.L. McEuen, *Phys. Rev. Lett.* **84**, 6082 (2000).
- [20] T. Ando and T. Nakashini, *J. Phys. Soc. Jpn.* **67**, 1704 (1998).
- [21] P.L. McEuen, M. Bockrath, D.H. Cobden, Y.G. Yoon, and S.G. Louie, *Phys. Rev. Lett.* **83**, 5098 (1999).
- [22] F. Triozon, S. Roche, A. Rubio, and D. Mayou, *Phys. Rev. B* **69**, 121410(R) (2004).
- [23] R. Avriller, S. Latil, F. Triozon, X. Blase, and S. Roche, *Phys. Rev. B* **74**, 121406(R) (2006).